The Astrophysical Journal, 838:27 (7pp), 2017 March 20 https://doi.org/10.3847/1538-4357/aa615a

Rotational Spectroscopy of the NH_3–H_2 Molecular Complex

L. A. Surin[1,2], I. V. Tarabukin[2], S. Schlemmer[1], A. A. Breier[3], T. F. Giesen[3], M. C. McCarthy[4,5], and A. van der Avoird[6]
[1] I. Physikalisches Institut, University of Cologne, Zülpicher Str. 77, D-50937 Cologne, Germany; surin@ph1.uni-koeln.de
[2] Institute of Spectroscopy of Russian Academy of Sciences, Fizicheskaya Str. 5, 108840 Troitsk, Moscow, Russia
[3] Institute of Physics, University of Kassel, Heinrich-Plett-Str. 40, D-34132 Kassel, Germany
[4] Harvard-Smithsonian Center for Astrophysics, Cambridge, MA 02138, USA
[5] Division of Engineering and Applied Sciences, Harvard University, Cambridge, MA 02138, USA
[6] Theoretical Chemistry, Institute for Molecules and Materials, Radboud University, Heyendaalseweg 135, 6525 AJ Nijmegen, The Netherlands
A.vanderAvoird@theochem.ru.nl
Received 2016 November 16; revised 2017 February 13; accepted 2017 February 15; published 2017 March 21

Abstract

We report the first high resolution spectroscopic study of the NH_3–H_2 van der Waals molecular complex. Three different experimental techniques, a molecular beam Fourier transform microwave spectrometer, a millimeter-wave intracavity jet OROTRON spectrometer, and a submillimeter-wave jet spectrometer with multipass cell, were used to detect pure rotational transitions of NH_3–H_2 in the wide frequency range from 39 to 230 GHz. Two nuclear spin species, (*o*)-NH_3–(*o*)-H_2 and (*p*)-NH_3–(*o*)-H_2, have been assigned as carriers of the observed lines on the basis of accompanying rovibrational calculations performed using the ab initio intermolecular potential energy surface (PES) of Maret et al. The experimental spectra were compared with the theoretical bound state results, thus providing a critical test of the quality of the NH_3–H_2 PES, which is a key issue for reliable computations of the collisional excitation and de-excitation of ammonia in the dense interstellar medium.

Key words: ISM: molecules – methods: laboratory: molecular – molecular data – molecular processes – techniques: spectroscopic

1. Introduction

The ammonia molecule is the most commonly used tracer of the temperature in a variety of interstellar environments, ranging from pre-stellar cores and molecular clouds to external galaxies (Ho & Townes 1983; Walmsley & Ungerechts 1983; Mauersberger et al. 2003; Mangum et al. 2013). These interstellar environments are usually far from thermodynamic equilibrium, and rotational excitation and de-excitation of the NH_3 molecules in collisions with H_2, the dominant colliding partner in most of the molecular regions, are of crucial importance for the observed ammonia population distributions and the interpretation of its spectra. Collisional state-to-state rates are difficult to measure experimentally, and as a result such information often relies on theoretical estimates based on potential energy surfaces (PESs). Laboratory measurements are important to establish the predictive abilities of these PESs. One of the most efficient tools for a reliable elucidation of intermolecular forces is high resolution spectroscopy of van der Waals complexes, because their (quasi)-bound states are very sensitive to the interaction potential (Wormer & van der Avoird 2000).

For NH_3–H_2, however, very little is known about its bound states. The high resolution infrared (IR) and microwave (MW) spectra of the related and isoelectronic HF–H_2 and H_2O–H_2 in the gas phase have been observed (Hunt et al. 2003; Weida & Nesbitt 1999; Harada et al. 2014), but no such data exist for ammonia. The available experimental studies of the NH_3–H_2 complex are limited to the observation of the ν_{HH} vibration (which is dipole forbidden in free H_2) in argon and neon matrices (Moroz et al. 1990; Jacox & Thompson 2006). In addition, ab initio calculations were performed in the latter work, which yielded a coaxial C_{3v} minimum energy arrangement and electronic dissociation energies of 215 and 237 cm^{-1} at the MP2 and CCSD(T) levels, respectively.

Not long ago, two high-accuracy ab initio five-dimensional PESs, including the anisotropy of H_2, were obtained for the NH_3–H_2 system using the coupled-cluster CCSD(T) method (Mladenović et al. 2008; Maret et al. 2009). In both studies the equilibrium structure of NH_3–H_2 was found to be axial, with molecular hydrogen collinear with the C_3 symmetry axis of ammonia. The H_2 monomer approaches NH_3 from the nitrogen side. This global minimum is bound by $D_e = 253\ cm^{-1}$ according to Mladenović et al. (2008) and 267 cm^{-1} according to Maret et al. (2009). The potential rises steeply for other H_2 orientations, indicating hindered internal rotation. The bond-dissociation energy D_0 was expected to be only a small fraction of D_e.

In the present paper, all bound rovibrational levels of the weakly bound NH_3–H_2 complex have been calculated for total angular momentum $J = 0...6$ on the intermolecular potential surface reported by Maret et al. (2009). The energy levels were obtained for four different nuclear spin states of NH_3–H_2 arising from combinations of (*para*)-H_2 and (*ortho*)-H_2 with (*ortho*)-NH_3 and (*para*)-NH_3. The (*p*)-H_2 and (*o*)-H_2 complexes and the (*o*)-NH_3 and (*p*)-NH_3 complexes behave as different molecules, because they do not interconvert at the timescale of the experiment, due to the different nuclear spin statistics.

The pure rotational (*end-over-end* rotation) spectra of two nuclear spin species—namely, (*o*)-NH_3–(*o*)-H_2 and (*p*)-NH_3–(*o*)-H_2—were detected in the frequency range of 39–230 GHz guided by the bound state calculations. The experimental data on the rotational levels are in good agreement with the theoretical results, which indicates the high quality of the PES used in this study.

2. Theory

2.1. Details on the Potential Surface

In our bound state calculations we applied the five-dimensional PES calculated ab initio by Maret et al. (2009).

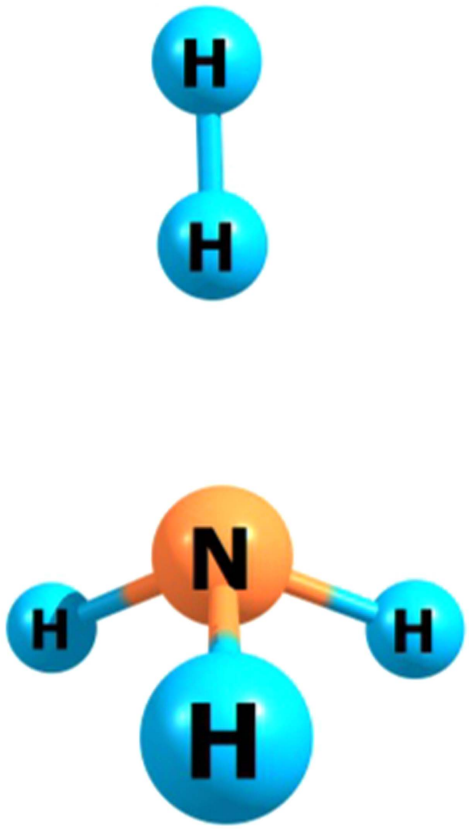

Figure 1. Most stable (global minimum) configuration of the NH_3–H_2 complex with C_{3v} symmetry. Distance between the centers of mass $R_e = 3.23$ Å, binding energy $D_e = 267\ cm^{-1}$ (Maret et al. 2009).

This potential depends only on the intermolecular coordinates, while the NH_3 and H_2 monomers were both kept rigid at their ground state vibrationally averaged geometries. Maret et al. constructed this PES by starting with a reference potential based on 89,000 data points from CCSD(T) calculations with Dunning's correlation consistent aug-cc-pVDZ basis set. In the next step, this reference PES was calibrated using a complete basis set extrapolation procedure on a smaller set of 29,000 data points from CCSD(T)/aug-cc-pVTZ calculations. The global minimum in the final potential deduced from an analytical fit to all data points has a depth D_e of 267 cm^{-1} and corresponds to a structure with intermolecular center-of-mass distance $R = 3.23$ Å and H_2 collinear with the C_{3v} axis of ammonia at the nitrogen end (see Figure 1). This PES has been employed in studies of collision dynamics of NH_3 with H_2 (Maret et al. 2009; Wiesenfeld et al. 2011; Pirani et al. 2013; Daniel et al. 2014; Ma et al. 2015; Tkáč et al. 2015).

2.2. Bound State Calculations

The rovibrational levels of NH_3–H_2 were calculated by a method similar to the coupled-channels method used in scattering calculations; it is described by van der Avoird and Nesbitt (2011). We used the ground state experimental values for the rotational constants of NH_3: $A_0 = B_0 = 9.9402\ cm^{-1}$ (298,000 MHz) and $C_0 = 6.3044\ cm^{-1}$ (189,001 MHz), given by Danby et al. (1986), and H_2: $B_0 = 59.3398\ cm^{-1}$ (1,778,962 MHz), given by Tkáč et al. (2015). The atomic masses are 1.007825 u for H and 14.003074 u for ^{14}N. For the intermolecular center-of-mass distance R, we used a discrete variable representation (DVR) with a grid of 95 equidistant points ranging from $R = 4$ to $26\,a_0$. This DVR basis was contracted into a radial basis of 20 functions constructed in the same way as in van der Avoird and Nesbitt (2011). To represent the hindered rotations of NH_3 and H_2 in the complex, we used a basis of symmetric rotor functions and spherical harmonics, respectively, which was truncated to internal rotor quantum numbers $j_{NH_3} \leqslant 10$ and $j_{H_2} \leqslant 6$. Wigner D-functions are used in the basis for the overall rotation of the dimer. With this basis, the bound levels of the complex are converged to better than 0.0001 cm^{-1}; the energies of transitions between the levels are converged even more accurately.

In order to explain the observed spectrum of NH_3–H_2, we must also include umbrella inversion tunneling of the NH_3 monomer in our calculations. The ground state inversion levels are split by 0.7934 cm^{-1} in the free monomer. Since the potential of Maret et al. (2009) does not depend on the umbrella inversion coordinate, we used a two-state model tested in previous work on NH_3–He (Gubbels et al. 2012) and NH_3–Ar (Loreau et al. 2014). It is assumed in this model that the NH_3 molecule tunnels between two structures, umbrella up and umbrella down, with an umbrella angle given by the equilibrium value in free ammonia. Maret et al. (2009) calculated their potential only for one of these structures; a symmetry relation (Gubbels et al. 2012) obeyed by the expansion coefficients of the potential yields its value for the umbrella-inverted structure. The basis for the rovibrational states of the complex is multiplied with two NH_3 inversion tunneling states, which according to the two-state model are the plus and minus combinations of the two localized umbrella states. NH_3 tunneling is partly quenched by the interaction with H_2 in the complex, and the tunneling states become more or less localized. The symmetry group used in the calculations is the permutation-inversion group G_{24}.

Due to the nuclear spin statistics of H_2, (p)-H_2 complexes with total nuclear spin $I_{H_2} = 0$ have their lowest internal rotor state with $j_{H_2} = 0$, while (o)-H_2 complexes with $I_{H_2} = 1$ have their lowest internal rotor state with $j_{H_2} = 1$, where j_{H_2} denotes the rotational angular momentum of H_2. The NH_3 part has also two nuclear spin states, (o)-NH_3 and (p)-NH_3, with the corresponding lowest rotational levels $(j_{NH_3}, k_{NH_3}) = (0, 0)$ and $(j_{NH_3}, k_{NH_3}) = (1, 1)$, where j_{NH_3} and k_{NH_3} denote the angular momentum of NH_3, and its projection on the symmetry axis.

Exact quantum numbers are the total angular momentum J of the complex and the parity $p = \pm 1$ under inversion E^*. It is conventional in spectroscopy to use the spectroscopic parity ε that is related to the inversion parity by $p = \varepsilon\,(-1)^J$. We follow this convention and label states of even/odd spectroscopic parity by e/f. An approximate quantum number that is important to understand the nature of the rovibrational states is the projection K of the total angular momentum J on the intermolecular axis. We also follow the convention to use the absolute value of K as a label, and distinguish the pairs of states with $K > 0$ by their parity e/f. States with $K = 0$ are called Σ states, those with $K = 1$ are Π states, and those with $K = 2$ are Δ states. Four different nuclear spin species occur in the complex: (o)-NH_3–(p)-H_2, (p)-NH_3–(p)-H_2, (o)-NH_3–(o)-H_2, and (p)-NH_3–(o)-H_2. For each of these species, we computed all bound rovibrational levels with total angular momentum $J = 0$–6 and both parities.

The rotational energy levels of NH_3–H_2 with $K = 0$ (Σ) and 1 (Π) are shown in Figure 2 for (p)-H_2 (left diagram) and (o)-H_2

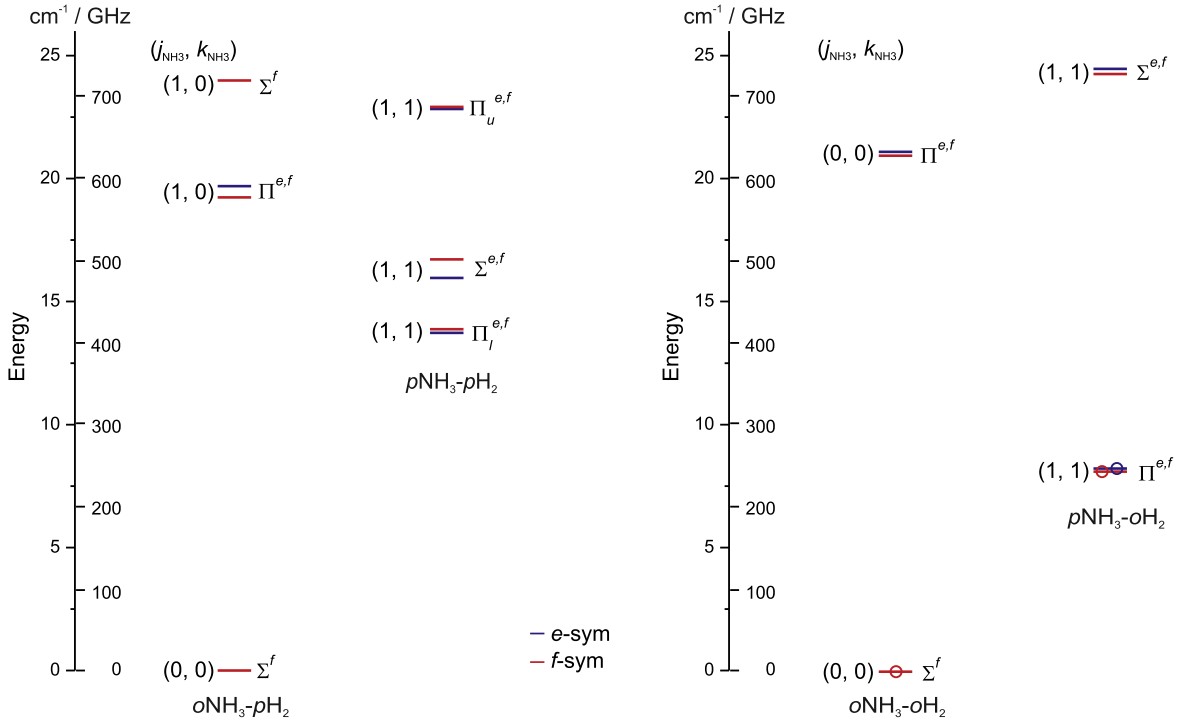

Figure 2. Calculated energy levels with $K = 0$ (Σ) and 1 (Π) for NH_3–(p)-H_2 (left) and NH_3–(o)-H_2 (right), up to 25 cm^{-1}. The relative position of the NH_3–(o)-H_2 and NH_3–(p)-H_2 energy scales is 91.33 cm^{-1}, as determined by the zero-point levels from the bound state calculations. (j, k) are quantum numbers of the correlating levels of free NH_3. Circles mean that *end-over-end* rotational transitions were observed within these states.

(right diagram). The zero of energies for NH_3–(p)-H_2 and NH_3–(o)-H_2 is simply fixed at the lowest $J = 0$ levels of the Σ ground states of the (o)-NH_3–(p)-H_2 and (o)-NH_3–(o)-H_2 complexes. The relative position of the NH_3–(o)-H_2 and NH_3–(p)-H_2 energy scales is 91.33 cm^{-1}, as determined by the zero-point levels of the complexes with (o)-H_2 and (p)-H_2 obtained from the bound state calculations.

Each level shown in Figure 2 involves a number of *end-over-end* rotational levels. The levels that belong to Σ states ($K = 0$) start at $J = 0$; levels that belong to Π states ($K = 1$) start at $J = 1$. The (p)-NH_3 dimers have a Π ground state with $J = 1$, and the (o)-NH_3 dimers have a Σ ground state with $J = 0$.

The bound state calculations yield different dissociation energies D_0 for the four nuclear spin species of the complex: 32.43, 34.25, 59.78, and 66.00 cm^{-1} for (o)-NH_3–(p)-H_2, (p)-NH_3–(p)-H_2, (o)-NH_3–(o)-H_2, and (p)-NH_3–(o)-H_2, respectively. Hence the dissociation energy D_0 is substantially larger for the (o)-H_2 dimers than for the (p)-H_2 dimers, while it is only slightly larger for the (p)-NH_3 dimers than for the (o)-NH_3 dimers. Similar stability differences among the (p)-H_2O–(p)-H_2, (o)-H_2O–(p)-H_2, (p)-H_2O–(o)-H_2, and (o)-H_2O–(o)-H_2 species were found for H_2O–H_2 by van der Avoird and Nesbitt (2011). It is also remarkable that D_0 is much smaller than the binding energy $D_e = 267\ cm^{-1}$ in the potential of Maret et al. (2009), which implies that the zero-point energy associated with the intermolecular vibrations and hindered rotations is large.

3. Experimental

Three different instruments, an intracavity OROTRON MMW spectrometer, a supersonic jet spectrometer for terahertz applications (SuJeSTa), and a Fourier transform microwave (FTMW) spectrometer were used to record the pure rotational spectrum of NH_3–H_2 in a jet expansion. Both OROTRON and FTMW spectrometers use an open Fabry–Perot cavity as a sample cell, and SuJeSTa uses a multipass cell, thus providing very high sensitivity, which is important for the detection of weakly bound van der Waals species. For most measurements, a gas mixture of 0.5%–1% of NH_3 in normal H_2 at a backing pressure of 4–6 bar was used to generate the NH_3–H_2 complexes in the molecular jet. In a few of the experiments, we used also neon or helium as a carrier gas. In all cases, the gas mixture adiabatically expanded into the cavity or multipass cell. The pulsed pinhole nozzle (General Valve, Series 9) of a 1 mm diameter operated at a repetition rate of 10–30 Hz. The accuracy of the measurements is about 100 kHz for MMW spectra and 2 kHz for FTMW spectra.

3.1. OROTRON Experiment

MMW spectra in the frequency range of 112–139 GHz were measured using the intracavity OROTRON spectrometer combined with a molecular jet expansion. This is a well-known technique (Surin et al. 2001) that has been used for more than 15 years for the observation of weakly bound complexes.

Briefly, the MMW generator OROTRON together with a pulsed supersonic jet is placed in a vacuum chamber. The free jet with a pulse duration of 500 μs enters the OROTRON resonant cavity perpendicularly to its axis. The high quality of the cavity ($Q \approx 10^4$) results in nearly 100 effective passes of the MMW radiation through the jet. Molecular absorption causes changes of the electron current in the OROTRON collector circuit and is detected by measuring these current changes. The radiation frequency of the OROTRON generator is modulated at 25 kHz, and phase sensitive detection of the absorption signal is achieved by a lock-in amplifier operated in 2f-mode. In addition, an on–off modulation of the jet is used for

baseline subtraction through a pair of gated integrators. Data averaging occurs within a time window of 1 ms. The double modulation technique substantially improves the signal-to-noise ratio. A small fraction of the OROTRON radiation is taken out from the cavity through coupling slits in the center of spherical mirror and mixed on a Schottky diode with the radiation of a MW synthesizer for frequency determination. The range of operation of the OROTRON tube used is 112–155 GHz, with a few small gaps. The double resonance method was applied for measurements at 75–80 GHz, outside the OROTRON frequency range. A MW synthesizer (Rohde & Schwarz, SMF100A) followed by wide-band amplifier and tripler (Virginia Diodes, Inc., AMC-S179/180) was used as a pump radiation source, giving relatively high output power (up to 10 mW).

3.2. SuJeSTA Experiment

The supersonic jet spectrometer for terahertz applications (SuJeSTA; Caris et al. 2009) has been applied for measurements of the NH_3–(*o*)-H_2 transitions at frequencies from 150 to 230 GHz. To obtain this frequency range, the 8–14 GHz output frequency of a synthesizer (Agilent 83650 B) is multiplied by a commercial multiplier chain (Virginia Diodes, Inc.). The resulting millimeter-wave radiation crosses a pulsed molecular jet approximately 5 cm downstream in a perpendicular position. Multipass optics (10 paths) is used to increase the signal-to-noise ratio. The absorption of radiation in the jet is detected by a low-noise liquid-He cooled InSb hot electron bolometer. The frequency of the synthesizer is modulated with a sine wave of 40 kHz, and phase sensitive detection of the signal is achieved by a lock-in amplifier operated in 2*f*-mode. Similar to the experiments with the OROTRON spectrometer, we used in addition to the frequency modulation of the radiation source an on–off modulation of the jet for baseline subtraction through a pair of gated integrators. Apart from substantially improving the signal-to-noise ratio, the double modulation technique suppresses standing wave etalon effects.

3.3. FTMW Experiment

The $J = 1$–0 line of (*o*)-NH_3–(*o*)-H_2 (Σ_f) near 39 GHz was measured at very high spectral resolution (0.1 ppm) with a high-Q FTMW spectrometer, the details of which are available elsewhere (McCarthy et al. 1997). The sample gas is injected through a pulsed pinhole nozzle into an evacuated Fabry–Perot resonator via a small hole in one of the cavity mirrors. A near resonant $\pi/2$ microwave pulse creates a macroscopic polarization of the molecular ensemble, and the resulting coherent emission signal is recorded as a function of time. Subsequently, Fourier transformation yields the frequency spectrum. Because the IF bandwidth of this spectrometer is very narrow, about 0.5 MHz, wide spectral searches are undertaken by synchronously changing the applied frequency and mirror separation under computer control. The (*o*)-NH_3–(*o*)-H_2 spectra at each setting of the cavity were averaged over 500 cycles at the 6 Hz repetition rate of the nozzle, using a gas sample consisting of about 0.5% NH_3 in 3–6 bar of normal H_2.

All observed transitions are Doppler-doubled, since the molecular beam travels parallel to the resonator axis. The full width at half-height for each line is 15 kHz, and the uncertainty in the line center frequencies is estimated to be ≈2 kHz.

At the extremely high resolution of the FTMW spectrometer, hyperfine structure due to the nuclear spin-spin and spin-rotation interactions of the H_2 part of the complexes is well resolved. The double resonance experiment was also performed to measure the $J = 2$–1 line of (*o*)-NH_3–(*o*)-H_2 (Σ_f) near 78 GHz, albeit with somewhat lower accuracy (20–50 kHz).

4. Observed Rotational Spectrum and Analysis

According to the bound states calculations (Section 2), the complexes of ammonia with (*o*)-H_2 are more strongly bound than those with (*p*)-H_2, and the formation of the NH_3–(*o*)-H_2 species in the molecular jet is more favorable. The initial search for rotational transitions was performed with the OROTRON spectrometer in the 115–118 GHz range, where the $R(2)$ line of (*o*)-NH_3–(*o*)-H_2 in the ground Σ_f state was predicted. One line was found at 117,789 MHz that is 1.3 GHz higher than the expected value. Then, the $R(1)$ transition was successfully detected at 78,836 MHz (about 900 MHz higher than the theoretical value) by the double resonance technique using the supposed $R(2)$ transition as a probe, thus confirming the assignment of both lines. The illustration of the double resonance recording is shown in Figure 3. In the same manner, two $R(2)$ transitions at 112 GHz and two $R(1)$ transitions at 75 GHz were detected and assigned for another spin modification, (*p*)-NH_3–(*o*)-H_2, in the Π_e/Π_f state.

These initial observations allowed a more accurate prediction of the higher-J transitions for the measurements with the SuJeSTA, in the frequency range from 150 to 230 GHz. The $R(3)$, $R(4)$, $R(5)$ transitions were detected for (*o*)-NH_3–(*o*)-H_2 in the ground Σ_f state, and the $R(3)$, $R(4)$ transitions for (*p*)-NH_3–(*o*)-H_2 in the Π_e/Π_f state.

Finally, the lowest $J = 1$–0 transition of (*o*)-NH_3–(*o*)-H_2 in the ground Σ_f state was measured near 39 GHz with the FTMW spectrometer. The observed line of (*o*)-NH_3–(*o*)-H_2 is split by the quadrupole interaction of the nitrogen nucleus ($I_N = 1$) into three hyperfine components, $F_1 = 1$–1, 2–1, and 0–1, and each component, except for $F_1 = 0$–1, is split further into three components due to the magnetic nuclear spin interaction of the H nuclei ($I_{H_2} = 1$), where F_1 and F denote the angular momenta $\boldsymbol{F}_1 = \boldsymbol{J} + \boldsymbol{I}_N$ and $\boldsymbol{F} = \boldsymbol{F}_1 + \boldsymbol{I}_{H_2}$, respectively. Applying the double resonance technique to the detected $R(0)$ transition, the $R(1)$ line of (*o*)-NH_3–(*o*)-H_2 (Σ_f) near 78 GHz was also observed. Six ^{14}N hyperfine components $F_1 = 2$–2, 1–0, 2–1, 3–2, 1–2, and 1–1 were resolved, which complements the initial measurement of the same rotational transition in the double resonance OROTRON experiment. All measured microwave and millimeter-wave transitions of the (*o*)-NH_3–(*o*)-H_2 and (*p*)-NH_3–(*o*)-H_2 complexes are listed in Table 1.

To analyze the observed spectra, we used an empirical energy expression for symmetric top molecules, in which the rotational energy including centrifugal distortion terms for each K-stack of levels were represented by a power series in $[J(J+1) - K^2]$:

$$E = B[J(J+1) - K^2] - D[J(J+1) - K^2]^2 + H[J(J+1) - K^2]^3 + L[J(J+1) - K^2]^4,$$

where $K = 0$ for the Σ states and $K = 1$ for the Π states. The quadrupole hyperfine interaction due to the N nucleus ($I_N = 1$) is given by

$$H_{eqQ} = (1/4)eqQ(3I_{Nz}^2 - \boldsymbol{I}_N^2),$$

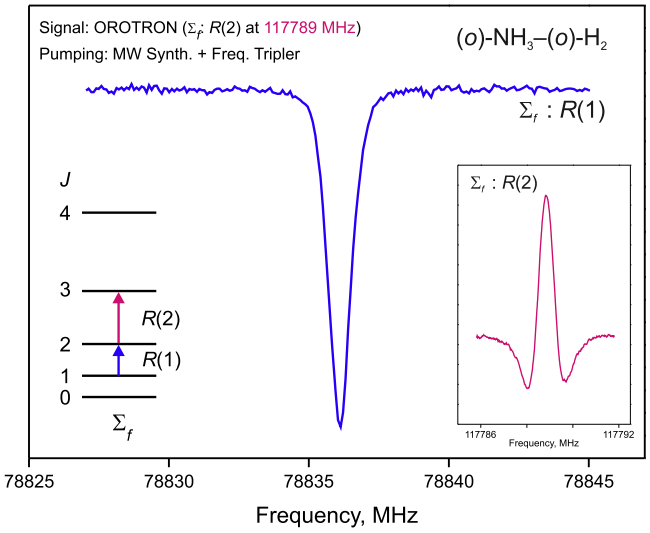

Figure 3. Double resonance recording of the $R(1)$ transition of the (o)-NH_3–(o)-H_2 complex in the ground Σ_f state using OROTRON spectrometer. The inset at the bottom right shows the signal $R(2)$ transition.

where $\boldsymbol{I}_N$ and I_{Nz} represent the nuclear spin of N and its projection on the intermolecular axis.

The hyperfine interaction of the H_2 unit (for (o)-H_2 species) originates from two sources, $H_{hfH} = H_{srH} + H_{ssH}$ (Kellogg et al. 1939, 1940). The first term H_{srH} denotes the interaction between the H nuclear spins and the rotation of the complex,

$$H_{srH} = -c\boldsymbol{I}_{H_2} \cdot \boldsymbol{J},$$

where I_{H_2} is the resultant nuclear spin of H_2 and c is the nuclear spin-rotation interaction constant. The second term H_{ssH} denotes the nuclear spin magnetic dipole–dipole interaction,

$$H_{ssH} = -\frac{5d}{(2J-1)(2J+3)}[3(\boldsymbol{I}_{H_2} \cdot \boldsymbol{J})^2 + (3/2)\boldsymbol{I}_{H_2} \cdot \boldsymbol{J} - \boldsymbol{I}_{H_2}^2 \cdot \boldsymbol{J}^2],$$

where d is the nuclear spin-spin interaction constant for NH_3–(o)-H_2.

The transitions of NH_3–H_2 assigned in this work were fitted using the PGOPHER program, which is open to the public (Western 2016). According to the corresponding measurement accuracies, the frequencies of the MMW and FTMW transitions were given weights of 1:50 in the fitting procedure. The double resonance frequencies measured with the FTMW spectrometer were included with a weight of 10. The results of the fit for NH_3–(o)-H_2 are given in Table 2, together with the rotational constants and hyperfine coupling constants determined from the theoretical energy levels and wave functions. The weighted value of the root mean squared deviation $\sigma_{fit} = 106$ kHz is close to our experimental uncertainty for the MMW data.

5. Discussion

The calculated positions of the lower states (<25 cm^{-1}) with $K = 0$ and 1 of the NH_3–H_2 complex that involve pure rotational transitions detected in the present work are shown in Figure 2. It was established in the bound state calculations and confirmed by the experiment that (o)-NH_3–(o)-H_2 has a ground state with $K = 0$ (Σ), while the ground state of (p)-NH_3–(o)-H_2 is a $K = 1$ (Π) state. The levels in Figure 2 are designated also by free internal rotor quantum numbers (j_{NH_3}, k_{NH_3}). Such a free internal rotor interpretation is of limited validity for NH_3–(o)-H_2, however, since analysis of the calculated wave functions shows that the j_{NH_3} values are strongly mixed by the anisotropic interaction potential. Thus the contributions of the (j_{NH_3}, k_{NH_3}) = (0, 0) and (1, 0) wave functions to the ground $K = 0$ (Σ) state of (o)-NH_3–(o)-H_2 are 51% and 43%. For the ground $K = 1$ (Π) state of (p)-NH_3–(o)-H_2, the contributions of the (j_{NH_3}, k_{NH_3}) = (1, 1) and (2, 1) wave functions are 86% and 13%.

The inversion tunneling motion of ammonia is nearly quenched for all states (Σ and Π levels) in (p)-NH_3–(o)-H_2. For the (p)-NH_3–(p)-H_2 species, the situation is somewhat different. The calculated splitting of the Σ levels is about 0.765 cm^{-1}, which is comparable with the value of the inversion splitting in free NH_3 (0.7934 cm^{-1}). Qualitatively, this picture is the same as observed and calculated for the NH_3–Ar complex (Zwart et al. 1991; Loreau et al. 2014), where the inversion motion of ammonia is hardly affected in the $\Sigma = 0$ states, while it is nearly quenched in the Π states. The reason that the inversion splittings are much smaller in NH_3–(o)-H_2 than in NH_3–(p)-H_2 is that the anisotropy of the intermolecular potential with respect to the orientation of H_2 is reflected by the interaction of NH_3 with (o)-H_2, whereas it is largely averaged out when NH_3 interacts with (p)-H_2.

In Tables 1 and 2 the measured transition frequencies and determined molecular parameters of (o)-NH_3–(o)-H_2 and (p)-NH_3–(o)-H_2 are compared with the results of bound state calculations. The theory predicts accurately the pure rotational transitions for the observed K-stacks, as can be seen by comparison, but the (Obs.–Calc.) deviations grow rapidly with increasing total angular momentum and amount to about +0.09 cm^{-1} at the maximum calculated value of $J = 6$. This indicates that the end-over-end rotational constant B from the calculations is too small by about 1%, which corresponds to the average distance R being too large by about 0.5%. A possible reason could be that the minimum in the intermolecular potential occurs slightly too far outward, because our calculations use the rigid monomer model, which may be somewhat inaccurate.

The average center-of-mass distances $\langle R \rangle$ are calculated to be 3.77 and 3.86 Å for (o)-NH_3–(o)-H_2 and (p)-NH_3–(o)-H_2, respectively, from the observed rotational constants, using the pseudo-diatomic approximation. The force constants for the vdW stretch vibration derived from the D_0 values are $k = 0.48$ and 0.61 N m^{-1}, while the vdW stretch frequencies are calculated to be 67.4 and 75.9 cm^{-1} for (o)-NH_3–(o)-H_2 and (p)-NH_3–(o)-H_2, respectively.

Dynamical information about the orientation of the ammonia unit within the van der Waals complex can be obtained from the determined quadrupole coupling constants using the expression $eqQ = (eqQ)_0 \langle P_2(\cos \vartheta_{NH_3}) \rangle$, where $(eqQ)_0$ is the quadrupole coupling constant for the free NH_3 molecule, −4.0898 MHz (Marshall & Muenter 1981), and ϑ_{NH_3} is the angle between the C_3 axis of NH_3 and the intermolecular axis. The expression assumes that complexation with the H_2 molecule has little effect on the electron distribution around the ^{14}N nucleus, and the angular brackets represent averaging over the internal motions of ammonia in the complex. Solving this expression for ϑ_{NH_3} yields two possible angles 42.°9/137.°1 for the Σ_f state of (o)-NH_3–(o)-H_2. The ab initio equilibrium structure value of $\vartheta_{NH_3} = 0°$ is closer to the first number. Such

Table 1
Observed Transitions of the NH_3–(*o*)-H_2 Complexes

State	$R(J)$	F_1'–F_1''	F'–F''	Obs., MHz	ab initio, MHz	O–C, MHz
(*o*)-NH_3–(*o*)-H_2						
		1–1	0–1	39509.3292		
			2–2, 1	39509.3755		
			1–2, 1, 0	39509.4033		
Σ_f	0	2–1	2–2, 1	39509.7223	39075	435
			3–2	39509.7682		
			1–2, 1, 0	39509.8194		
		0–1	1–2, 1, 0	39510.3292		
		2–2		78835.675		
		1–0		78835.750		
		2–1		78836.070		
	1	3–2		78836.100	77963	873
		1–2		78836.335		
		1–1		78836.688		
	2			117788.840	116468	1321
	3			156162.250	154380	1782
	4			193724.900	191458	2267
	5			230202.040	227418	2784
(*p*)-NH_3–(*o*)-H_2						
Π_e	1			75107.670	74111	997
	2			112334.830	110843	1491
	3			149133.940	147149	1985
	4			185303.095	182819	2484
	5			⋯	217586	⋯
Π_f	1			75344.840	74362	983
	2			112683.715	111212	1472
	3			149589.305	147628	1961
	4			185860.795	183406	2455
	5			⋯	218281	⋯

Table 2
Molecular Parameters for the NH_3–(*o*)-H_2 Complexes (All Values in MHz)

		Experiment	ab initio
(*o*)-NH_3–(*o*)-H_2	B	19770.01615(54)	19562.12
Σ_f	D	7.56561(19)	8.40
	H	$-8.920(13) \times 10^{-3}$	
	L	$-3.537(21) \times 10^{-5}$	
	eQq	−1.2510(21)	−1.10
	c	$-5.36(76) \times 10^{-3}$	
	d	$24.29(46) \times 10^{-3}$	22.49
(*p*)-NH_3–(*o*)-H_2	B	18808.346(24)	18578.13
Π_e	D	5.145(2)	6.29
	H	$-1.773(4) \times 10^{-2}$	
Π_f	B	18868.354(38)	18640.32
	D	5.274(3)	6.35
	H	$-1.622(6) \times 10^{-2}$	

a comparison, however, has to be made very cautiously, since the values of the nuclear quadrupole coupling constants are highly averaged quantities.

The Legendre polynomial factor $\langle P_2(\cos\vartheta_{NH_3})\rangle$ in the previous equation will be zero if the ammonia subunit undergoes free internal rotation. For (*o*)-NH_3–(*o*)-H_2, it is 0.306, a value that is remarkably large in comparison to −0.066 for the Ne–(*o*)-NH_3 (van Wijngaarden & Jäger 2001) and −0.086 for Ar–(*o*)-NH_3 (Nelson et al. 1986) complexes. This suggests a more hindered internal motion of NH_3 in the (*o*)-NH_3–(*o*)-H_2 complex. The different sign of $\langle P_2(\cos\vartheta_{NH_3})\rangle$ for (*o*)-NH_3–(*o*)-H_2 assumes an "on average" more parallel orientation of NH_3 to the intermolecular axis, in contrast to more perpendicular in case of Ar– and Ne–(*o*)-NH_3. The theoretical $\langle P_2(\cos\vartheta_{NH_3})\rangle$ factor (0.268) obtained from the calculated ground Σ_f state wave functions of (*o*)-NH_3–(*o*)-H_2 and the corresponding angle (44.°3) agree well with experiment (0.306; 42.°6).

The magnetic nuclear spin interaction parameters of the H nuclei in *o*-H_2 provide information about the average orientation of the hydrogen molecule with the complex. The hyperfine coupling constant d determined for (*o*)-NH_3–(*o*)-H_2 is 24.29 kHz, while the d_H value for the free H_2 molecule is reported to be 57.671 kHz from molecular beam experiments (Harrick et al. 1953). The equation $d = d_H\langle P_2(\cos\vartheta_{H_2})\rangle$, where ϑ_{H_2} is the angle between the H_2 bond and the intermolecular axis can be used to estimate the average value $\langle P_2(\cos\vartheta_{H_2})\rangle$, which is sensitive to the internal rotation state of H_2. The derived $\langle P_2(\cos\vartheta_{H_2})\rangle$ value of 0.42 for (*o*)-NH_3–(*o*)-H_2 is almost equal to 0.4 expected for uniaxial free rotation (Yu et al. 2005; Harada et al. 2014). It is also worth noting that the hyperfine coupling constant inferred from our study (d = 24.29 kHz) is very close to the value of 24.68 kHz determined earlier for the (*p*)-H_2O–(*o*)-H_2 molecular complex (Harada et al. 2014). The theoretical $\langle P_2(\cos\vartheta_{H_2})\rangle$ factor (0.39) obtained from the calculated ground Σ_f state wave functions of (*o*)-NH_3–(*o*)-H_2 agrees well with experiment (0.42).

Unfortunately, we were unable in the present study to detect the pure rotational transitions in the Σ and Π states of the (p)-H_2 nuclear spin species (shown in Figure 2, left). This is not surprising with the use of normal hydrogen, because NH_3 complexes containing (o)-H_2 bind significantly stronger than those with (p)-H_2. Also, in H_2O–H_2 spectra reported by van der Avoird & Nesbitt (2011), the (p)-H_2 complexes could not be observed, and a similar stability difference between the complexes of H_2O with (p)-H_2 and (o)-H_2 was found from ab initio calculations. The absence of the (p)-H_2 species was explained in this paper in more detail by a kinetic mechanism. Moreover, for the (p)-H_2 complex, the dipole moment may be averaged out to a larger extent because of a more nearly free rotation of NH_3 in the complex. It seems that an enriched sample of (p)-H_2 is necessary for the production and observation of the (o)-NH_3–(p)-H_2 and (p)-NH_3–(p)-H_2 complexes.

6. Conclusions

This paper describes the first observation of the pure rotational spectrum of the NH_3–H_2 complex and a calculation of the rovibrational bound states on a 5D intermolecular potential surface obtained through high-level ab initio calculations. The observed transitions were assigned to two nuclear spin species, (o)-NH_3–(o)-H_2 and (p)-NH_3–(o)-H_2. These data were included in a fit to determine a set of empirical molecular parameters for both (o)-NH_3–(o)-H_2 and (p)-NH_3–(o)-H_2. All bound rovibrational levels of the four nuclear spin species were computed for total angular momentum $J = 0$–6.

A significant fraction of the NH_3–H_2 binding energy goes into the zero-point energy associated with the intermolecular vibrations and internal rotations: the dissociation energies D_0 are 32.43, 34.25, 59.78, and 66.00 cm^{-1} for (o)-NH_3–(p)-H_2, (p)-NH_3–(p)-H_2, (o)-NH_3–(o)-H_2, and (p)-NH_3–(o)-H_2, respectively. The computed energy levels were compared with the rotational spectra measured in the present work. We found good agreement with the experiment for all detected stacks, although we noted a systematic increase of the rotational energy differences with increasing J, which indicates that the calculated end-over-end rotational constant of the complex is too small by about 1%. The reason for the latter deviation may be the use of a rigid monomer model.

Finally, we conclude that the present results provide a considerable amount of new information, both experimental and theoretical, which elucidates the intermolecular interactions and dynamics in the astrophysically relevant NH_3–H_2 system.

We would like to thank Dr. F. Lewen for his assistance with double resonance experiment using OROTRON spectrometer and Dr. C. Western for implementation of nuclear spin-spin interactions in the PGOPHER fitting program. This work was partly supported by Deutsche Forschungsgemeinschaft (DFG) via SFB 956 and Russian Foundation for Basic Research (RFBR) through grants 15-03-09333 and 16-33-00616.

References

Caris, M., Giesen, T. F., Duan, C., et al. 2009, JMoSp, 253, 99
Danby, G., Flower, D. R., Kochanski, E., et al. 1986, JPhB, 19, 2891
Daniel, F., Faure, A., Wiesenfeld, L., et al. 2014, MNRAS, 444, 2544
Gubbels, K. B., van de Meerakker, S. Y. T., Groenenboom, G. C., Meijer, G., & van der Avoird, A. 2012, JChPh, 136, 074301
Harada, K., Tanaka, K., Kubota, H., & Okabayashi, T. 2014, CPL, 605-606, 67
Harrick, N. J., Barnes, R. G., Bray, P. J., & Ramsey, N. F. 1953, PhRv, 90 260
Ho, P. T. P., & Townes, C. H. 1983, ARA&A, 21, 239
Hunt, S. W., Higgins, K. J., Craddock, M. B., Brauer, C. S., & Leopold, K. R. 2003, JAChS, 125, 13951
Jacox, M. E., & Thompson, W. E. 2006, JChPh, 124, 204304
Kellogg, J. M. B., Rabi, I. I., Ramsey, Jr., N. F., & Zacharias, J. R. 1939, PhRv, 56, 728
Kellogg, J. M. B., Rabi, I. I., Ramsey, Jr., N. F., & Zacharias, J. R. 1940, PhRv, 57, 677
Loreau, J., Liévin, J., Scribano, Y., & van der Avoird, A. 2014, JChPh, 141, 224303
Ma, Q., van der Avoird, A., Loreau, J., et al. 2015, JChPh, 143, 044312
Mangum, J. G., Darling, J., Henkel, C., et al. 2013, ApJ, 779, 33
Maret, S., Faure, A., Scifoni, E., & Wiesenfeld, L. 2009, MNRAS, 399, 425
Marshall, M. D., & Muenter, J. S. 1981, JMoSp, 85, 322
Mauersberger, R., Henkel, C., Weiß, A., Peck, A. B., & Hagiwara, Y. 2003, A&A, 403, 561
McCarthy, M. C., Travers, M. J., Kovacs, A., Gottlieb, C. A., & Thaddeus, P. 1997, ApJS, 113, 105
Mladenović, M., Lewerenz, M., Cilpa, G., Rosmus, P., & Chambaud, G. 2008, CP, 346, 237
Moroz, A., Sweany, R. L., & Whittenburg, S. L. 1990, JPhCh, 94, 1352
Nelson, D. D., Fraser, G. T., Peterson, K. I., et al. 1986, JPhCh, 85, 5512
Pirani, F., Cappelletti, D., Belpassi, L., & Tarantelli, F. 2013, JPCA, 117, 12601
Surin, L. A., Dumesh, B. S., Lewen, F., et al. 2001, RScI, 72, 2535
Tkáč, O., Saha, A. K., Loreau, J., et al. 2015, MolPh, 113, 3925
van der Avoird, A., & Nesbitt, D. J. 2011, JChPh, 134, 044314
van Wijngaarden, J., & Jäger, W. 2001, JChPh, 115, 6504
Walmsley, C. M., & Ungerechts, H. 1983, A&A, 122, 164
Weida, M. J., & Nesbitt, D. J. 1999, JChPh, 110, 156
Western, C. M. 2016, JQRST, 186, 221
Wiesenfeld, L., Scifoni, E., Faure, A., & Roueff, E. 2011, MNRAS, 413, 509
Wormer, P. E. S., & van der Avoird, A. 2000, ChRv, 100, 4109
Yu, Z., Higgins, K. J., Klemperer, W., McCarthy, M. C., & Thaddeus, P. 2005, JChPh, 123, 221106
Zwart, E., Linnartz, H., Meerts, W. L., et al. 1991, JChPh, 95, 793